Using the Distribution Theory to Simultaneously Calibrate the Sensors of a Mobile Robot

Agostino Martinelli

INRIA

INSTITUT NATIONAL DE RECHERCHE EN INFORMATIQUE ET EN AUTOMATIQUE

Using the Distribution Theory to Simultaneously Calibrate the Sensors of a Mobile Robot

Agostino Martinelli

N° 6796

Janvier 2009

Thèmes COG et NUM

ISSN 0249-6399 ISRN INRIA/RR--6796--FR+ENG

INSTITUT NATIONAL
DE RECHERCHE
EN INFORMATIQUE
ET EN AUTOMATIQUE

INRIA

centre de recherche
GRENOBLE – RHÔNE-ALPES

Using the Distribution Theory to Simultaneously Calibrate the Sensors of a Mobile Robot

Agostino Martinelli

Thèmes COG et NUM — Systèmes cognitifs et Systèmes numériques
Équipe-Projet Emotion

Rapport de recherche n° 6796 — Janvier 2009 — 36 pages

Abstract: This document considers the problem of sensor self-calibration in mobile robotics by only using a single point feature. In particular, it is introduced a simple and efficient strategy to extrinsically calibrate a bearing sensor (e.g. a vision sensor) mounted on a vehicle and simultaneously estimate the parameters describing the systematic error of its odometry system. Special attention is devoted to investigate the dependence of the observability properties of these parameters on the chosen robot trajectory. The document provides two contributions. The first one is the analytical derivation of the combinations of these parameters which are observable for a given robot trajectory. This derivation requires to perform a local decomposition of the system, based on the theory of distributions. In this respect, this document represents the first application of the distribution theory in the frame-work of mobile robotics. Then, starting from this decomposition, it is possible to analytically derive the expression of the bearing angle of the feature in the bearing sensor local frame vs the curve length of the robot trajectory as evaluated by the odometry. Starting from this expression, a method to efficiently estimate the parameters describing both the extrinsic bearing sensor calibration and the odometry calibration is derived (second contribution). Many accurate simulations and real experiments with the robot e-Puck equipped with encoder sensors and a camera show the robustness the efficiency and the accuracy of the proposed approach.

Key-words: Distribution Theory, Non Observability, Calibration, Mobile Robotics

Centre de recherche INRIA Grenoble – Rhône-Alpes
655, avenue de l'Europe, 38334 Montbonnot Saint Ismier
Téléphone : +33 4 76 61 52 00 — Télécopie +33 4 76 61 52 52

Application de la Théorie des Distributions pour Calibrer les Capteurs d'un Robot Mobile

Résumé : Ce document considère un problème d'auto calibration pour les capteurs d'un robot mobile en utilisant une seule amère. En particulier, il sera introduit une technique très efficace et performante pour calibrer les paramètres extrinsèques d'un capteur capable de donner les angles de vue d'une amère (une camera) et au même temps les paramètres qui donnent la calibration d'un system odomètre. Le document introduit deux nouvelles contributions. La première est l'application de la théorie des distributions pour étudier l'observabilité du problème. La deuxième est la technique de calibration. Ce document contient aussi une validation de la technique soit avec des simulations soit avec expérimentations réels avec le robot mobile e-puck.

Mots-clés : Théorie des distributions, Non observabilité, Calibration, Robots Mobiles

1 Introduction

A sensor calibration technique is a method able to estimate the parameters characterizing the systematic error of the sensor. In mobile robotics, performing this process autonomously is not only a desire which automatizes a work which would have to be performed by hand, but it is in many cases a real need for application-like scenarios. This is especially true for the odometry. Indeed, the pressure of tires can change over time and the effective wheel diameters depend also on the robot load. Having a system able to adapt continuously to different floor types and changing wheels attributes (i.e. different tire pressure, deterioration, etc.) is a key advantage. In order to fully achieve this objective, a calibration strategy must be able to operate in a completely unknown environment by only using the data coming from the robot sensors and hopefully even when these data are able to get very little information about the surroinding environment (e.g. when these data only consist of the bearing angle of a single feature). On the other hand, when a mobile robot is equipped with more than one sensor, another significant source of systematic error comes from a poor knowledge about the transformation among the reference frames attached to the sensors. In several cases, estimating this transformation by hand provides very poor results. This for instance holds for vision sensors where the exact position of the principal point is unknown. Therefore, methods able to perform this estimation by only using the data provided by the sensors themselves must be considered.

1.1 Previous Works

Several strategies have been developed to perform sensor calibration.

Regarding the odometry, a very successful strategy has been introduced in 1996 by Borenstein and Feng [4]. This is the UMBmark method. It is based on absolute robot position measurements after the execution of several square trajectories.

Several strategies have also been introduced to simultaneously estimate the robot configuration and the parameters characterizing the systematic odometry error both for indoor (e.g. [13], [15]) and outdoor environments [6]. They are based on an Extended Kalman Filter. In [10] also the mapping problem was considered.

In [14] the problem of also estimating the non-systematic odometry errors was considered. More recently, a method based on two successive least-squares estimations has been introduced [1]. In this case, the least-square approach was justified by the linear relation between the parameters to be estimated and the measurements. In particular, this linear link is not the result of a linearization.

All these approaches exhibit very good performance. However, they rely on an a priori knowledge of the environment or on the possibility to perform absolute robot position measurements, for instance by equipping the robot with a GPS. Very few approaches calibrate the odometry without the need of an a priori knowledge of the environment and/or of the use of global position sensors (like a GPS). One of these methods is described in [20] where the estimation of the kinematic calibration parameters is carried out by comparing consecutive laser scans. Also the approach introduced in [8], called the Path Comparison

(PC) method, does not need a priori knowledge of the environment and/or global position sensors. In particular, in [8] it has been used the generalized Voronoi graph (GVG) to force the robot to follow a known path: the robot is forced to follow a path along the GVG and track the same path but in the reverse direction, not using the odometry information. Finally, in [21] an automatic calibration method for a multisensor system has been introduced. Also in this case the calibration is carried out by exploiting the redundancy of information provided by the robot sensors.

Regarding the problem of sensor to sensor calibration, several cases have recently been considered (e.g. IMU-camera [19], laser scanner-camera [5], [22], [23] and odometry-camera [16]).

In [16], an observability analysis taking into account the system nonlinearities was also provided to understand whether the system contains the necessary information to perform the self calibration. Indeed, a necessary condition to perform the estimation of a state, is that the state is observable. In [16] it was investigated whether the state containing the extrinsic parameters of the vision sensor is or is not observable. The *observability rank criterion* introduced by Hermann and Krener [11] was adopted to this scope. The same observability analysis was later applied to the case of the odometry self-calibration [17]. However, in these works, what it was determined is only whether the state containing the parameters defining the sensor systematic error is observable or not. On the other hand, when a state is not observable, suitable combinations of its components could be observable and therefore could be estimated. The derivation of these combinations is very important in order to properly exploit the information contained in the sensor data to estimate a given set of parameters. This derivation requires to perform a local decomposition [12]. While in the linear case this decomposition is easy to be performed, in the non linear case it is often troublesome and requires to apply the theory of distributions developed in [12]. In practice, the solution of partial differential equations has to be computed.

1.2 Contributions

In this document we consider the case when the calibration is carried out by only using a single point feature. In particular, we consider the simultaneous self calibration of the odometry system and the extrinsic calibration of a bearing sensor. To the best of our knowledge this problem has never been investigated before.

The document provides two contributions:

- A local decomposition of the considered system based on the theory of distributions developed in [12];
- A new strategy to robustly, efficiently and accurately estimate the parameters describing both the extrinsic bearing sensor calibration and the odometry calibration.

The first contribution was also discussed in our very recent work [18]. To the best of our knowledge this contribution represents the first application of the distribution theory in the field of mobile robotics and the first non-trivial

application of this theory to face a real estimation problem. In the specific case, it allows us to detect for suitable trajectories the observable combinations of the original parameters describing all the error systematic components (i.e. the estimation of the reference change between the bearing sensor and the odometry system and the odometry calibration).

By carrying out this decomposition for suitable circular trajectories, it is possible to analytically derive the expression of the bearing angle of the feature in the bearing sensor local frame vs the curve length of the robot trajectory as evaluated by the odometry. For circular trajectories this expression is a periodic function of the curve length. The structure of this function depends also on the observable combinations previously derived. In particular, by analytically analyzing this function it is possible to detect symmetry properties which play a very practical importance. Indeed, by only evaluating the axis of symmetry of this function and its period it is possible to immediately evaluate the observable combinations. Then, by performing at least three independent circular trajectories, it is possible to evaluate all the parameters describing our calibration problem.

Section 2 defines the calibration problem and provides the basic equations to characterize the system dynamics and the observation. In section 3 we remind some results from the theory developed in [11] (3.1) and [12] (3.2). In section 4 we perform the decomposition for circular robot trajectories. This allows us to detect the combinations of the parameters which are observable. Then, in section 5, we analytically derive the relation between the observation (consisting of the bearing angle of the feature in the local frame of the bearing sensor) and the curve length as evaluated by the encoders. Based on this analytical expression we derive fundamental properties of this function (section 6) and, based on them, we introduce the calibration strategy in section 7. Finally, we evaluate its performance in section 8, with simulations (8.1) and real experiments (8.2). Conclusions are provided in section 9.

2 The Considered System

We consider a mobile robot moving in a $2D$-environment. The configuration of the robot in a global reference frame can be characterized through the vector $[x_R, y_R, \theta_R]^T$ where x_R and y_R are the cartesian robot coordinates and θ_R is the robot orientation. The dynamics of this vector are described by the following non-linear differential equations:

$$\begin{cases} \dot{x}_R = v\cos\theta_R \\ \dot{y}_R = v\sin\theta_R \\ \dot{\theta}_R = \omega \end{cases} \tag{1}$$

where v and ω are the linear and the rotational robot speed, respectively. The link between these velocities and the robot controls (u) depends on the considered robot drive system. We will consider the case of a differential drive. In order to characterize the systematic odometry error we adopt the model introduced in [4]. We have:

$$v = \frac{\delta_R v_R + \delta_L v_L}{2} \qquad \omega = \frac{\delta_R v_R - \delta_L v_L}{\delta_B B} \tag{2}$$

where v_R and v_L are the control velocities (i.e. $u = [v_R, v_L]^T$) for the right and the left wheel, B is the nominal value for the distance between the robot wheels and δ_R, δ_L and δ_B characterize the systematic odometry error due to an uncertainty on the wheels diameters and on the distance between the wheels.

Furthermore, a bearing sensor (e.g. a camera) is mounted on the robot. We assume that its vertical axis is aligned with the $z-$axis of the robot reference frame and therefore the transformation between the frame attached to this sensor and the one of the robot is characterized through the three parameters ϕ, ρ and ψ (see fig. 1).

The available data are the control $u = [v_R, v_L]^T$ and the bearing angle of a single feature (β in fig. 1) at several time steps during the robot motion.

We introduce the following quantities:

$$\theta \equiv \theta_R - atan2(y_R, x_R); \quad \gamma \equiv \theta + \phi; \tag{3}$$
$$\mu \equiv \frac{\rho}{D} \equiv \frac{\rho}{\sqrt{x_R^2 + y_R^2}}$$

By using simple trigonometry algebra we obtain (see also fig. 1):

$$\beta = \begin{cases} -atan\left(\dfrac{\sin\gamma}{\mu + \cos\gamma}\right) - \psi + \pi & if\ \gamma_- \le \gamma \le \gamma_+ \\ -atan\left(\dfrac{\sin\gamma}{\mu + \cos\gamma}\right) - \psi & otherwise \end{cases}$$

where γ_- and γ_+ are the two solutions (in $[-\pi, \pi)$) of the equation $\cos\gamma = -\mu$ with $\gamma_+ = -\gamma_-$ and $\gamma_+ > 0$. We made the assumption $0 < \mu < 1$ since we want to avoid collisions between the robot and the feature ($D > \rho$).

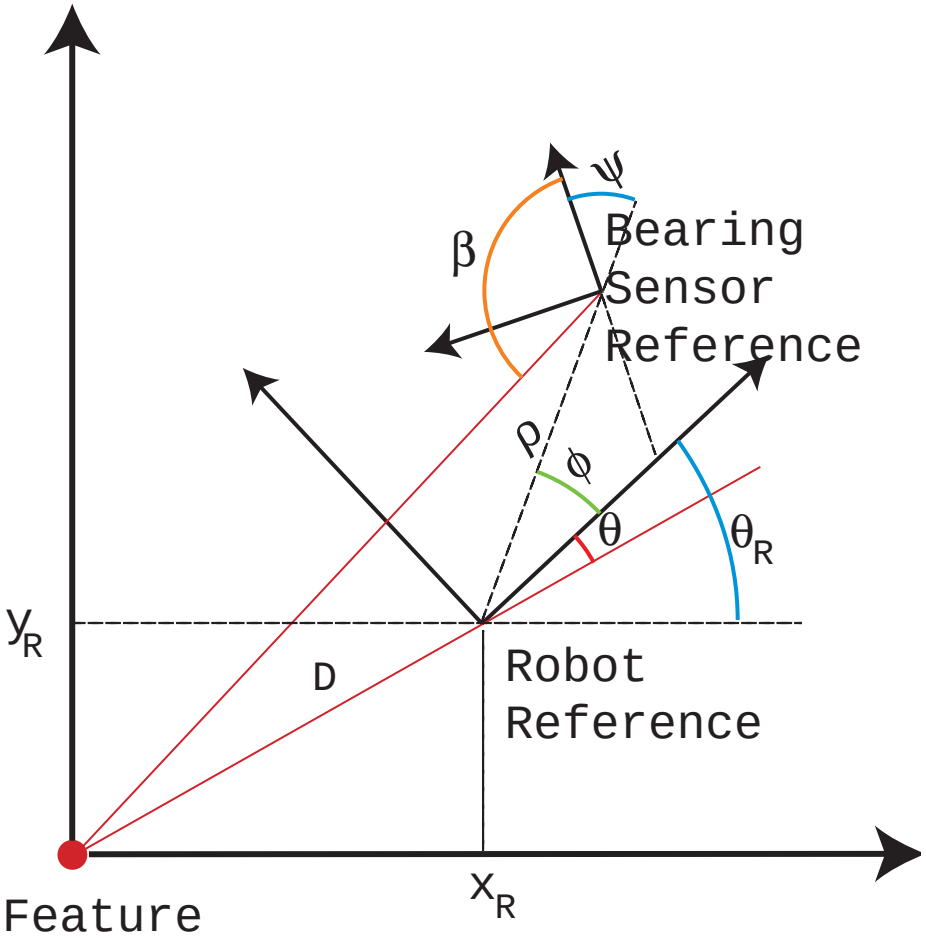

Figure 1: The two reference frames respectively attached to the robot and the bearing sensor.

By using (1) and the definitions in (3) the dynamics of our system is described by the following equations:

$$\begin{cases} \dot{\mu} = -\mu^2 \dfrac{v}{\rho} \cos(\gamma - \phi) \\ \dot{\gamma} = \omega - \mu \dfrac{v}{\rho} \sin(\gamma - \phi) \\ \dot{\phi} = \dot{\rho} = \dot{\psi} = \dot{\delta}_R = \dot{\delta}_L = \dot{\delta}_B = 0 \end{cases} \tag{4}$$

The goal is to estimate simultaneously the parameters ϕ, ρ, ψ, δ_R, δ_L and δ_B using the available data (i.e. v_R, v_L and β in a given time interval). Since these data consists of angle measurements (the wheel diameters are not known and in fact are to be estimated), the best we can hope is the possibility to estimate these parameters up to a scale factor. In particular, we will refer to the following parameters:

$$\phi, \quad \psi, \quad \eta \equiv \frac{\delta_R}{2\rho}, \quad \delta \equiv \frac{\delta_L}{\delta_R}, \quad \xi \equiv \frac{1}{B}\frac{\delta_R}{\delta_B} \tag{5}$$

The dynamics and the observation of our system is described by the following equations:

$$\begin{cases} \dot{\mu} = -\mu^2 \eta (v_R + \delta v_L) \cos(\gamma - \phi) \\ \dot{\gamma} = \xi(v_R - \delta v_L) - \mu\eta(v_R + \delta v_L) \sin(\gamma - \phi) \\ \dot{\phi} = \dot{\psi} = \dot{\eta} = \dot{\delta} = \dot{\xi} = 0 \\ \beta = \begin{bmatrix} -atan\left(\dfrac{\sin\gamma}{\mu + \cos\gamma}\right) - \psi + \pi & \gamma_- \le \gamma \le \gamma_+ \\ -atan\left(\dfrac{\sin\gamma}{\mu + \cos\gamma}\right) - \psi & otherwise \end{bmatrix} \end{cases} \tag{6}$$

In section 4 we derive for circular trajectories, which combinations of μ, γ, ϕ, ψ, η, δ and ξ are observable and hence can be estimated. Then, in sections 5, 6 and 7 we introduce a very efficient strategy to estimate these parameters. Finally, by adding a simple metric measurement (e.g. the initial distance between the robot and the feature) the original parameters ϕ, ρ, ψ, δ_R, δ_L and δ_B can also be estimated.

The dynamics in (6) has the following structure:

$$\dot{X} = f(X, u) = \sum_{i=0}^{2} f_i(X) u_i \tag{7}$$

where: $X = [\mu,\ \gamma,\ \phi,\ \psi,\ \eta,\ \delta,\ \xi]^T$, $u_1 = v_R$, $u_2 = v_L$ and

$$\begin{aligned} f_1 &= -\left[\mu^2 \eta \cos(\gamma - \phi), \mu\eta \sin(\gamma - \phi) - \xi, 0, 0, 0, 0, 0\right]^T \\ f_2 &= -\delta\left[\mu^2 \eta \cos(\gamma - \phi), \mu\eta \sin(\gamma - \phi) + \xi, 0, 0, 0, 0, 0\right]^T \end{aligned} \tag{8}$$

3 Observability Properties and Local Decomposition

In control theory, a system is defined as observable when it is possible to reconstruct its initial state by knowing, in a given time interval, the control inputs and the outputs [12]. The observability property has a very practical meaning. When a system is observable it contains all the necessary information to perform the estimation with an error which is bounded [12].

3.1 Observability Rank Criterion

In a nonlinear system the concept of *local distinguishability* was introduced by Hermann and Krener [11]. The same authors introduced also a criterion, the *observability rank criterion*, to verify whether a system has this property. This criterion plays a very important role since in many cases a nonlinear system, whose associated linearized system is not observable, has however the local distinguishability property. Regarding the localization problem this was proven in [2] and [3]. Note that it is the distinguishability property telling us that the system contains the necessary information to have a bounded estimation error (actually, provided that the locality is large enough with respect to the sensor accuracy).

We now want to remind some concepts in the theory by Hermann and Krener in [11]. We will adopt the following notation. We indicate the K^{th} order Lie derivative of a field Λ along the vector fields $v_{i_1}, v_{i_2}, ..., v_{i_K}$ with $L^K_{v_{i_1},v_{i_2},...,v_{i_K}}\Lambda$. Note that the Lie derivative is not commutative. In particular, in $L^K_{v_{i_1},v_{i_2},...,v_{i_K}}\Lambda$ it is assumed to differentiate along v_{i_1} first and along v_{i_K} at the end.

Let us indicate with Ω the space spanned by all the Lie derivatives $L^K_{f_{i_1},f_{i_2},...,f_{i_K}}\beta|_{t=0}$ $(i_1, i_2, ..., i_K = 1, 2$ and the functions f_{i_j} are defined in (8).

Furthermore, we denote with $d\Omega$ the space spanned by the gradients of the elements of Ω.

In this notation, the observability rank criterion can be expressed in the following way: *The dimension of the observable sub-system at a given X_0 is equal to the dimension of $d\Omega$.*

We adopt this criterion to investigate the observability properties of our system when the robot moves along circular trajectories. In particular, we evaluate the dimension of $d\Omega$. Since this dimension is smaller than the dimension of the entire configuration space, we perform a local decomposition of the system to detect which combinations of the state are observable.

3.2 Local Decomposition

Let us suppose that a given system is not observable. We refer to the case where the dynamics have the structure as in (7) but with a single input control. Indeed, in the next section we consider circular robot trajectories, i.e. trajectories with only one degree of freedom. By denoting the state with S, we can describe the system by the following equations:

$$\begin{cases} \dot{S} = f(S)u, \quad S \in \mathbb{R}^n \\ y = h(S) \end{cases} \tag{9}$$

where y is the output (observation) of the system (in our case $y = \beta \in \mathbb{R}$)

We are assuming that S is not observable, i.e. the dimension of the associated subspace $d\Omega$ is smaller than n (in this case the Lie derivatives are computed only along the vector field $f(S)$). Let us suppose that this dimension is equal to n_{obs}. According to the theory of distributions developed in [12], we can find n_{obs} independent combinations of the components of the original state S which are observable and $n - n_{obs}$ independent combinations of the components of S which are not observable. More precisely, if we include the n_{obs} observable combinations in the vector S_2 and the other $n - n_{obs}$ combinations in the vector S_1, we have the following decomposition for the original system:

$$\begin{cases} \dot{S}_1 = f_1(S_1, S_2)u \\ \dot{S}_2 = f_2(S_2)u \\ y \ = h_2(S_2) \end{cases} \tag{10}$$

In particular, the subsystem defined by the last two equations in (10) is independent of the value of S_1 and it is observable. Therefore, by performing this decomposition, we can use the information coming from the dynamics (i.e. the knowledge of $u(t)$) and the observations ($y(t)$) in order to estimate the observable quantities (S_2). This decomposition is very important in every estimation problem when the state is not observable. Indeed, estimating directly the original state S results in an erroneous evaluation.

In section 2, when we introduced the two quantities defined in (3) and the three parameters η, δ, ξ, we performed such a decomposition for the state $[x_R,\ y_R,\ \theta_R,\ \phi,\ \rho,\ \psi,\ \delta_R,\ \delta_L,\ \delta_B]^T$: indeed, the new state $[\mu,\ \gamma,\ \phi,\ \psi,\ \eta,\ \delta,\ \xi]^T$ is observable as proven in appendix A and its components are non linear combinations of the components of the original state (which is not observable). On the other hand, in the most of cases it is very troublesome to perform such a decomposition. In the next section we perform such a decomposition for the same state (i.e. $[\mu,\ \gamma,\ \phi,\ \psi,\ \eta,\ \delta,\ \xi]^T$) but when we only allow the robot to move along circular trajectories. We apply the distributions theory developed in [12].

4 Local Decomposition for Circular Trajectories

We consider the one-degree of freedom motion obtained by setting $v_R = \nu$, $v_L = q\nu$.

Let us define:

$$\eta_q \equiv \eta(1 + q\delta) \quad \xi_q \equiv \xi(1 - q\delta) \tag{11}$$

From the dynamics in (6) we obtain the following dynamics:

$$\begin{cases} \dot{\mu} &= -\mu^2 \eta_q \nu \cos(\gamma - \phi) \\ \dot{\gamma} &= \xi_q \nu - \mu \eta_q \nu \sin(\gamma - \phi) \\ \dot{\eta}_q = \dot{\xi}_q = \dot{\phi} = \dot{\psi} &= 0 \end{cases} \tag{12}$$

In appendix B we provide the steps necessary to perform the local decomposition of this system. Here we give the solutions. Let us define:

$$\Psi_1^q \equiv \frac{\xi_q - \eta_q \sin\phi}{\eta_q \cos\phi}, \quad \Psi_2^q \equiv \frac{\mu \eta_q \cos\phi}{\sin\gamma},$$
$$\Psi_3 \equiv \frac{\mu + \cos\gamma}{\sin\gamma} \tag{13}$$

The local decomposition is:

$$\begin{cases} \dot{A}^q = \nu(1 + A^{q^2})(\xi_q - V^q) \\ \dot{V}^q = \nu A^q V^q (2V^q - \xi_q) \\ \dot{L}^q = \dot{\xi}_q = 0 \\ \beta \ = -atanA^q - L^q + S_p \dfrac{\pi}{2} \end{cases} \tag{14}$$

where:

$$A^q \equiv \frac{\Psi_1^q - \Psi_3}{1 + \Psi_1^q \Psi_3}, \quad V^q \equiv \Psi_2^q \frac{1 + \Psi_1^q \Psi_3}{1 + \Psi_3^2},$$
$$L^q \equiv \psi - atan\Psi_1^q \tag{15}$$

and S_p can be ± 1 depending on the values of the system parameters. We do not provide here this dependence. In the next section we will investigate some important properties of S_p vs the robot motion.

Deriving this decomposition is very hard. As shown in appendix B, it requires to solve two partial differential equations. However, to check the validity of this decomposition is very simple since it only requires to compute derivatives (e.g. this can be done by using the matlab symbolic functions). Furthermore, also the solution has a simple analytical expression.

This decomposition has a very practical importance. It tells us that, when the robot accomplishes circular trajectories, the information contained in the sensor data (i.e. the information contained in the function $\nu(t)$ and $\beta(t)$) allows us to estimate only the state $[A^q,\ V^q,\ L^q,\ \xi_q]^T$ and not the original state $[\mu,\ \gamma,\ \phi,\ \psi,\ \xi,\ \delta,\ \eta]^T$. In the next sections we will provide a powerful strategy to estimate the initial value $[A_0^q,\ V_0^q,\ L^q,\ \xi_q]^T$ for a given circular trajectory. Then, by combining at least three independent circular trajectories (i.e. with a different q) it is possible to perform the calibration.

5 Deriving an Analytical Expression for the Observation Function

For the sake of simplicity in the next sections we neglect the suffix q on the three parameters A, V and L. On the other hand, to distinguish ξ_q from ξ previously defined, we still maintain q in ξ_q.

By integrating the first two equations in (14) we obtain:

$$\frac{(1+A^2)V^2}{2V-\xi_q} = k \tag{16}$$

The parameter k is related to the initial values:

$$k = \frac{(1+A_0^2)V_0^2}{2V_0-\xi_q} \tag{17}$$

From (16) we obtain the two expressions

$$AV = \pm\sqrt{k(2V-\xi_q)-V^2} \tag{18}$$

By substituting this expression in the second equation of (14) and by solving the differential equation we obtain the solutions:

$$V = \frac{\xi_q k(2k-\xi_q) + kw^2 \pm w\sqrt{k(k-\xi_q)(w^2+\xi_q^2)}}{(2k-\xi_q)^2+w^2} \tag{19}$$

where:

$$w = \xi_q \tan(c \pm \xi_q s) \tag{20}$$

$$c = atan\left(\frac{\xi_q k + (\xi_q - 2k)V_0}{\xi_q\sqrt{-V_0^2+2kV_0-\xi_q k}}\right) \tag{21}$$

and

$$s = s(t) = \int_0^t \nu(\tau)d\tau \tag{22}$$

By using (18) and the last equation in (14) we get the following expressions for the output β:

$$\beta = \pm atan\left(\sqrt{\frac{k(2V-\xi_q)-V^2}{V^2}}\right) - L + S_p\frac{\pi}{2}$$

The previous expressions provide more than one solution for the observation β. Our goal is to have a unique expression of the observation function for every value of s. To achieve this result we need to investigate the continuity properties for the derived expressions (see next section).

Let us introduce the following three sign variables: S_w, S_V, and S_y. As for S_p, each one can assume the value of $+1$ or -1. The analytical expression of the observation function β vs s is provided by the following equations:

$$w = \xi_q \tan(c + S_w\xi_q s) \tag{23}$$

$$V = \frac{\xi_q k(2k - \xi_q) + kw^2 + S_V w\sqrt{k(k - \xi_q)(w^2 + \xi_q^2)}}{(2k - \xi_q)^2 + w^2} \tag{24}$$

$$\beta = S_y atan\left(\sqrt{\frac{k(2V - \xi_q) - V^2}{V^2}}\right) - L + S_p\frac{\pi}{2} \tag{25}$$

In particular, we note that β depends on s through the function w which is a periodic function whose period is $\frac{\pi}{|\xi_q|}$.

The expression of the observation given in (23-25)) depends also on the observable parameters $A_0,\ V_0,\ L,\ \xi_q$. A_0 and V_0 appear in the previous expressions through k and c (see equations (17) and (21)). Actually, instead of A_0 and V_0 it is easier to directly refer to k and c. By having the measurements $y(t)$ and $\nu(t)(= \dot{s}(t))$ we have the information to estimate the state $[L,\ \xi_q,\ k,\ c]^T$. In the next section we derive a fundamental theorem which allows us to estimate this state very efficiently.

6 Continuity Properties for the Observation Function

This section consists of two parts. In the first one we investigate the continuity properties of the observation function in order to derive how the sign variables depend on the curve length. Then, we derive a theoretical result which has a very practical importance. Indeed, it allows us to efficiently estimate the state $[L,\ \xi_q,\ k,\ c]^T$ for a given circular trajectory (defined by a given q).

When we investigate the continuity properties for the observation function and its first derivative it is possible to detect two kind of points. We call them *Nodes* and *k-Nodes*.

6.1 Nodes

We define the nodes as the points where w diverges. From (23) it is easy to find their values:

$$s_n = -S_w \frac{c}{\xi_q} + j\frac{\pi}{\xi_q} + S_w \frac{\pi}{2\xi_q} \tag{26}$$

j being an integer. In other words, there are infinite nodes at the distance of $\frac{\pi}{|\xi_q|}$ one each other.

It holds the following important result: *In order to have the continuity of the observation function on the nodes the value of S_V must flip in correspondence of each node.*

To prove the previous result it is sufficient to compute the left and the right limit of V on the nodes. By using the expression in (24) and assuming $\xi_q > 0$ it is easy to get:

$$\lim_{c+S_w\xi_q s \to \frac{\pi}{2}^- + j\frac{\pi}{\xi_q}} V = \lim_{w\to+\infty} V = k + S_V\sqrt{k(k-\xi_q)}$$

$$\lim_{c+S_w\xi_q s \to \frac{\pi}{2}^+ + j\frac{\pi}{\xi_q}} V = \lim_{w\to-\infty} V = k - S_V\sqrt{k(k-\xi_q)}$$

They coincide when the value of S_V flips in correspondence of the node. When $\xi_q < 0$ the first limit $c + S_w\xi_q s \to \frac{\pi}{2}^- + j\frac{\pi}{\xi_q}$ corresponds to $w \to -\infty$ and the second limit $c + S_w\xi_q s \to \frac{\pi}{2}^+ + j\frac{\pi}{\xi_q}$ corresponds to $w \to +\infty$. Therefore, the same result holds.

Furthermore, by considering the first derivative of the observation function we obtain the result: *In order to have the continuity of the the first derivative of the observation function on the nodes the value of S_y must flip in correspondence of each node.*

To prove this it is sufficient to consider the first derivative of the function $\sqrt{\frac{k(2V-\xi_q)-V^2}{V^2}}$ and compute once again the right and the left limit on the nodes.

By combining the previous two results we obtain:

Property 1 (Node Continuity) *In order to have the continuity of the the observation function and its first derivative on the nodes the values of S_V and S_y must flip in correspondence of each node.*

6.2 k-Nodes

We define the k-nodes as the points where $V = 0$. Starting from the expression in (24) it is possible to find that these points exist if and only if $-k\xi_q \geq 0$. In this case we obtain:

$$s_{kn} = -S_w \frac{c}{\xi_q} + j\frac{\pi}{\xi_q} - \frac{S_w S_V}{\xi_q} atan\left(\sqrt{-\frac{k}{\xi_q}}\right) \tag{27}$$

The observation function is continuous on the k-nodes without flipping the sign variables. However, in order to have continuity on its first derivative, S_y must flip. On the other hand, if only S_y flips we loose the continuity of the observation function. To have the continuity on both the observation function and its derivative both S_y and S_p must flip. We therefore have the following property:

Property 2 (k-Node Continuity) *In order to have the continuity of the the observation function and its first derivative on the k-nodes S_y and S_p must flip in correspondence of each k-node .*

6.3 Mirror Points

We define these points with the following expression:

$$s_{mp} = -S_w \frac{c}{\xi_q} + j\frac{\pi}{\xi_q} \tag{28}$$

for every integer j. From this definition it is easy to verify that $w(s_{mp}) = 0$. Furthermore, from (26) and (27) we have:

$$s_n = s_{mp} + S_w \frac{\pi}{2\xi_q} \tag{29}$$

$$s_{kn} = s_{mp} - \frac{S_w S_V}{\xi_q} atan\left(\sqrt{-\frac{k}{\xi_q}}\right) \tag{30}$$

In Fig 2 we represent all the previous points. In particular, fig 2*a* refers to the case when the k-nodes do not exist ($k\xi_q > 0$). We assumed $S_w = 1$ and, for the sake of clarity, we assumed $S_V = S_y = S_p = 1$ on the right of the first indicated node. In both cases we observe that the values of S_V, S_y and S_p are all together again the same by increasing s of $2\frac{\pi}{|\xi_q|}$. Since $\frac{2\pi}{|\xi_q|}$ is a multiple of the period of w, this means that the observation function is a periodic function with the period:

$$T_S = \frac{2\pi}{|\xi_q|} \tag{31}$$

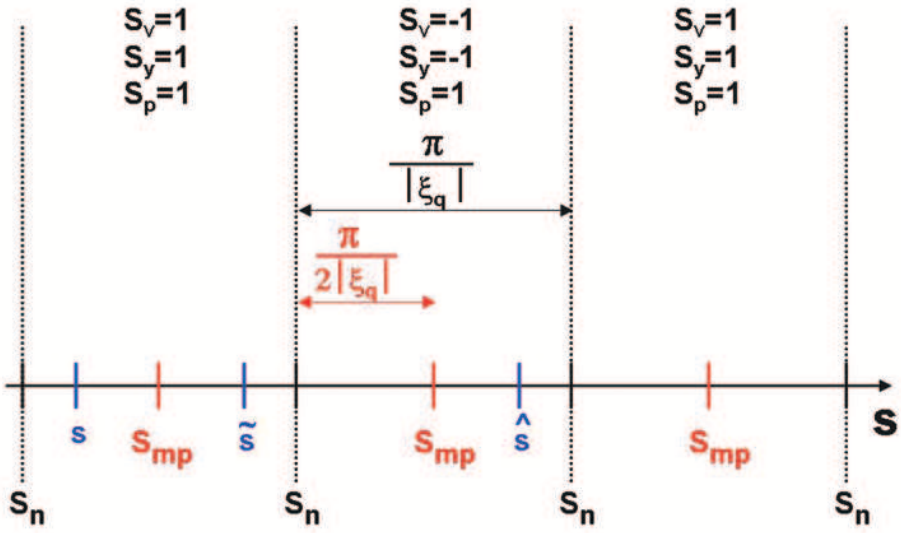

a

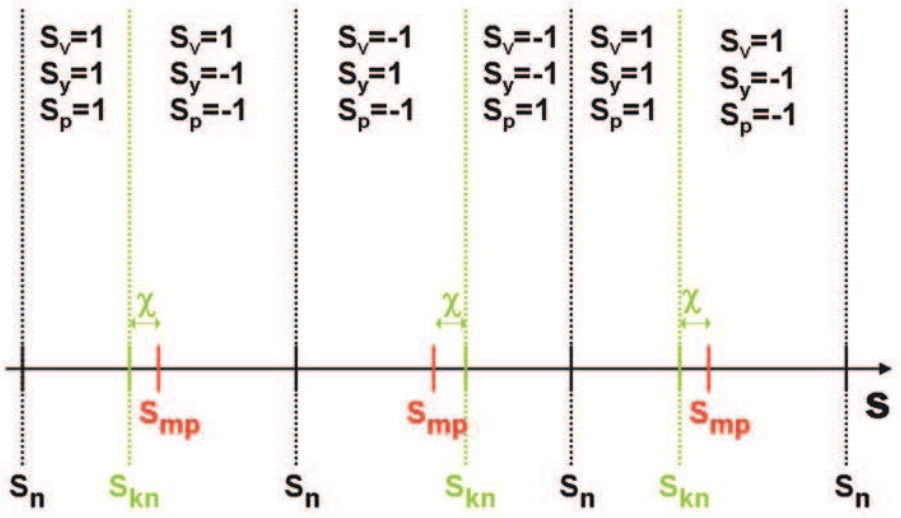

b

Figure 2: Special points where the sign variables change their value. *a* illustrates the case when k-nodes do not exist and *b* when they exist. In *a* also the shift and reflection operations on a generic point s are shown.

6.4 Shift and Reflection

Let us consider a generic point s. We define two operations. The first one, called *shift*, associates to s the value:

$$\overline{s} \equiv s + \frac{T_S}{2} \tag{32}$$

The second one is called *reflection*. By indicating with s^R_{mp} the closest mirror point to s on the right, the reflection associates to s the point $\widetilde{s}$ which is the symmetric point of s with respect to s^R_{mp} (see fig 2*a* for an illustration). From this definition we have $s + \widetilde{s} = 2s^R_{mp}$, i.e.:

$$\widetilde{s} \equiv 2s^R_{mp} - s \tag{33}$$

It is easy to verify that the operations of shift and reflection are commutative. We will indicate with $\hat{s}$ the point obtained when these two operations are both applied on s (i.e. $\hat{s} \equiv \widetilde{\overline{s}}$). By indicating with s^R_n the closest node to s on the right, it results that $\hat{s}$ is the symmetric point of s with respect to s^R_n (see fig 2*a* for an illustration), namely:

$$\hat{s} = 2s^R_n - s \tag{34}$$

6.5 The Effect of Shift and Reflection on the Observation Function

In the previous subsection we defined the operation of shift and reflection on a given point s. We define the same operations on a given function $f(s)$ as the ones associating to $f(s)$ the value of the function f calculated respectively in $\overline{s}$ and $\widetilde{s}$.

Lemma 1 (Reflection and Shift on w) *The function w changes its sign when the operation of reflection is applied, namely $w(\widetilde{s}) = -w(s)$. Furthermore, since w is invariant to the shift (indeed it is a periodic function with period equal to $\frac{T_S}{2}$), it also changes sign when both the reflection and the shift are applied, i.e. $w(\hat{s}) = -w(s)$*

Proof: From (33) we have $w(\widetilde{s}) = w(2s^R_{mp} - s)$. On the other hand, s^R_{mp} is a mirror point, i.e. satisfies the equation (28) for a given integer j (which depends on s). Hence, $w(\widetilde{s}) = w(2s^R_{mp} - s) = w\left(-2S_w \frac{c}{\xi_q} + 2j\frac{\pi}{\xi_q} - s\right)$. Finally, by using (23) we obtain $w\left(-2S_w \frac{c}{\xi_q} + 2j\frac{\pi}{\xi_q} - s\right) = \xi_q \tan\left(-c - S_w \xi_q s\right) = -w(s)$.

Lemma 2 (Nodes and k-Nodes Layout) *For every s, between s and $\hat{s}$ there is one and only one node and, in the case when the k-nodes exist, there are either zero or two k-nodes.*

Proof: From (34) we know that s and $\hat{s}$ are symmetric with respect to the closest node on the right of s. This means that this and only this node is between them. On the other hand, when the k-nodes exist, they are also symmetric with respect to the nodes (see fig 2*b* and the equations (28-30)). Hence, between s and $\hat{s}$ there are either zero or two k-nodes.

Lemma 3 (Reflection and Shift on the Sign Variables) *We have the following equations:* $S_w(\hat{s}) = S_w(s)$, $S_V(\hat{s}) = -S_V(s)$, $S_y(\hat{s}) = -S_y(s)$ *and* $S_p(\hat{s}) = S_p(s)$

Proof: Regarding S_w we know from the previous continuity analysis that it does not change with s and hence it is independent of the shift and reflection. Regarding the other sign variables, the previous equations are a direct consequence of the lemma 2 and the properties 1 and 2.

Theorem 1 (Reflection and Shift on the Observation Function) *The observation function satisfies the following fundamental equation* $\forall s$*:*

$$\beta(s) + \beta(\hat{s}) = -2L \ (\mod \pi) \tag{35}$$

Proof: Let us consider a point s. By explicating the dependence on s, the observation function in (25) is:

$$\beta(s) = Q(s) - L + S_p(s)\frac{\pi}{2}$$

with $Q(s) = S_y(s)\ atan\left(\sqrt{\frac{k(2V(s)-\xi_q)-V(s)^2}{V(s)^2}}\right)$. On the other hand, from lemmas 1 and 3 and the equation (24) it is immediate to verify that $V(\hat{s}) = V(s)$. Therefore, from lemma 3 we obtain:

$$\beta\left(\hat{s}\right) = -Q(s) - L + S_p(s)\frac{\pi}{2}$$

By summing up the two previous expressions it is immediate to get (35).

7 The Strategy to Estimate the System Parameters

The results derived in the previous section allow us to immediately evaluate the parameters ξ_q, L, k and c for a single circular trajectory.

Equation (31) allows us to estimate the parameter ξ_q by evaluating the period of the observation function. Actually, this equation does not provide the sign of ξ_q. However, this sign is positive for all the values of $q < \frac{1}{\delta}$ (i.e. when the robot accomplishes counter clock-wise circular trajectories).

Once ξ_q is estimated, the next step consists in the evaluation of the position of one node. Indeed, once we know the position of one node, we can determine c (or better few candidates of c) by using (26). On the other hand, the position of one node can be evaluated by using the previous theorem (i.e. the equation (35). The algorithm 1 describes the procedure to perform this evaluation. It computes the left hand side of equation (35), called $\theta(s_c, s)$, for every possible node candidate (s_c), which is in the interval $[0, \frac{T_S}{2}]$. The function $\theta(s_c, s)$ is independent of the second argument s when $s_c = s_n$. Indeed, $\theta(s_n, s) = -2L \ \forall s$. This means that the standard deviation of $\theta(s_c, s)$ respect to the second argument (s) is zero when computed in s_n (i.e. $\sigma(s_n) = 0$). When the robot sensors are affected by measurement errors, the function $\sigma(s_c)$ attains its minimum on s_n, as illustrated in figures 5*c* and 5*d*.

Algorithm 1 (Returns one Node)
for $s_c = 0$ *to* $\frac{T_S}{2}$ ***do***
  for $s = 0$ *to* $\frac{T_S}{2}$ ***do***
    $\hat{s} = 2s_c - s$
    $\theta(s_c, s) = \beta(s) + \beta(\hat{s})(\mod \pi)$
  end for
end for
for $s_c = 0$ *to* $\frac{T_S}{2}$ ***do***
  $\sigma(s_c) =$ *standard deviation of* $\theta(s_c, s)$
end for
$s_n = \arg min_{s_c} \sigma(s_c)$

Once s_n is determined, equations (34) and (35) allow us to immediately evaluate the parameter L. Furthermore, as said before, equation (26) allows us to evaluate c. In both cases few possible values for these parameters are actually provided. The correct ones can be selected by combining more than one circular trajectory. On the other hand, combining at least three trajectories (with different q) is necessary also to estimate our original parameters ϕ, ψ, η, δ and ξ once the parameters ξ_q and L are evaluated for each trajectory.

Regarding the parameter k its value can be estimated from the following expression:

$$k = \frac{\xi_q}{1 - \tan^2\left(\frac{\beta(m_1) - \beta(m_2)}{2}\right)} \tag{36}$$

where m_1 and m_2 are the positions of two consecutive mirror points (both m_1 and m_2 are independent of k). The previous expression is obtained starting

from (23-25), by observing that the function w is zero on the mirror points and by observing that when the shift and reflection are applied on a mirror point we obtain the next mirror point (i.e. $\hat{m}_1 = m_2$). Then by using lemmas 2 and 3 we obtain (36).

We remark that the parameters ξ_q, L and c can be estimated by using all the available measurements. In contrast, k is obtained by using two measurements. This results in a rough estimation of k when the sensor measurements are significantly noisy. On the other hand, the estimation of all the four parameters can be refined by applying a bundle adjustment technique after the previous first evaluation is done (this first evaluation is very important to avoid local minima). In our experiments we adopted the Levenberg Marquadt algorithm. However, regarding ξ_q and L the correction introduced by this refinement is negligible.

Once the parameters ξ_q and L are estimated for at least three independent trajectories (i.e. corresponding to three different values of q, q_1, q_2 and q_3), the calibration parameters ϕ, ψ, η, δ and ξ can be found by using (11), the first equation in (13) and the last equation in (15).

In particular, by having the value of ξ_q for two trajectories, it is possible to get the parameters ξ and δ by using the second equation in (11). Then, by using (11) and the first in (13) we obtain the following equation:

$$\eta_x \Psi_1^q + \eta_y = f_q$$

where $\eta_x \equiv \eta \cos\phi$, $\eta_y \equiv \eta \sin\phi$ and $f_q \equiv \xi \frac{1+q\delta}{1-q\delta}$. By using two distinct trajectories (corresponding to q_1 and q_2), we can solve the linear system

$$\begin{bmatrix} \Psi_1^{q_1} & 1 \\ \Psi_1^{q_2} & 1 \end{bmatrix} \begin{bmatrix} \eta_x \\ \eta_y \end{bmatrix} = \begin{bmatrix} f_{q_1} \\ f_{q_2} \end{bmatrix}$$

where $\Psi_1^q = \tan(\psi - L^q)$. In this way we obtain both η_x and η_y in terms of ψ. By using the third equation $\eta_x \Psi_1^{q_3} + \eta_y = f_{q_3}$ we can compute ψ.

As said in section 2, the information provided by the sensor data only allows us to estimate the parameters ϕ, ψ, η, δ and ξ, i.e. the calibration parameters up to a scale factor. However, by adding a supplementary metric measurement we can also estimate the original parameters ϕ, ρ, ψ, δ_R, δ_L and δ_B. Let us suppose to have the initial distance of the robot from the feature for only one among the three trajectories. Let us suppose that it is the trajectory defined by $q = q_1$. Once the parameters ϕ, ψ, η, δ and ξ are estimated as previously explained, we consider also the parameters c and k for the trajectory with $q = q_1$. By using (17) and (21) we obtain the values of A_0 and V_0. Then, by using the first two equations in (15) we obtain the corresponding Ψ_2^q and Ψ_3^q at $s = 0$. From the last two equations in (13) we obtain the initial values γ_0 and μ_0. On the other hand, having the initial distance D_0 allows us to obtain $\rho = \mu_0 D_0$. Once ρ is evaluated we can estimate $\delta_R = 2\rho\eta$ and then $\delta_L = \delta\delta_R$ and $\delta_B = \frac{\delta_R}{B\xi}$.

r	B	K	ν
$0.3m$	$0.5m$	$0.001m^{\frac{1}{2}}$	$0.05ms^{-1}$

Table 1: The parameters characterizing the simulated odometry system.

8 Performance Evaluation

In order to carefully evaluate the proposed strategy we performed both simulations and real experiments.

8.1 Simulations

The dynamics of the simulated robot are described by the equations (1) and (2). The robot is equipped with encoder sensors able to provide the rotations of the right and the left wheel occurred at every time step. These encoder data are delivered at $50Hz$. Furthermore, accordingly with the model introduced in [7], all these measurements are affected by zero mean Gaussian errors independent among them. In particular, according with the error model in [7], the variance of each measurement is proportional to the value provided by the sensor. In other words, let us suppose that the true rotations of the right and left wheel occurred at a given time step are equal to $\delta\alpha_R^{true}$ and $\delta\alpha_L^{true}$. We generate the following measurements:

$$\delta\alpha^R = N\left(\delta\alpha_R^{true}, \frac{K_R^2}{r_R}|\delta\alpha_R^{true}|\right)$$

$$\delta\alpha^L = N\left(\delta\alpha_L^{true}, \frac{K_L^2}{r_L}|\delta\alpha_L^{true}|\right)$$

where $N(m, \sigma^2)$ indicates the normal distribution with mean value m and variance σ^2, r_R and r_L are respectively the nominal values of the radius of the right and left wheel, and K_R and K_L characterize the non systematic odometry error. We considered many different values for the parameters characterizing the simulated odometry system (i.e. K_R, K_L, r_R, r_L, the robot speed ν and the distance between the wheels (B) appearing in (2)). The precision of our strategy is always excellent, even when we considered values of K_R and K_L much larger (hundred times) than the values obtained through real experiments (see [7] where $K_R \simeq K_L \simeq 5\ 10^{-4} m^{\frac{1}{2}}$).

In this section we provide a part of the results obtained with our simulations. In particular, we set $r \equiv r_R = r_L$, $K \equiv K_R = K_L$. In table 1 we report the parameters characterizing the robot dynamics. Observe that the chosen K is larger than the experimental values provided in [7], i.e. we are simulating encoder sensors more inaccurate and this is more challenging for the performance of our strategy.

The simulated exteroceptive sensor provides the bearings of a single feature at the origin. These data are delivered at $1Hz$. Furthermore, we assume that these bearing measurements are affected by a zero mean Gaussian error. In other words, when at a give time step the true bearing of the feature in the local frame of the sensor is β^{true} we generate the following measurement:

ϕ	ρ	ψ	δ_R	δ_L	δ_B
$0.0000deg$	$0.30000m$	$90.000deg$	0.99000	1.0060	0.97000

Table 2: The true values of the calibration parameters adopted in our simulations

$$\beta = N(\beta^{true}, \sigma_\beta^2)$$

We performed many simulations by varying the value of σ_β in the range $[0, 5]deg$.

Finally, we considered many values for the calibration parameters: ϕ, ρ, ψ, δ_R, δ_L and δ_B. However, the performance of our strategy does not depend on them. For this reason, we show here a single case. Tables 2 provide the values of the calibration parameters adopted in the simulations here reported.

Figure 3 reports the results obtained in the ideal case when both the odometry and the bearing sensor are noise-less (i.e. $\sigma_\beta = K = 0$). In particular, we show two cases corresponding to have the observed feature inside and outside the accomplished circular trajectory. The motion is characterized by $q = 0.8$ and the other parameters have the values previously specified. The robot trajectories and the feature are displayed in figure $3a$ and $3b$, respectively. Figures $3c$ and $3e$ show respectively the observation function with the two nodes (red stars) and the function $\sigma(s_c)$ for the motion shown in figure $3a$. s_c is the supposed position of one node. When s_c is equal to the true node position the function $\sigma(s_c)$ attains its minimum. In this case this minimum is equal to zero since it refers to an ideal case. Figures $3d$ and $3f$ refer to the case shown in figure $3b$.

Figure 4 displays the results obtained by setting $\sigma_\beta = 1deg$ and the value of K specified in table 1. In this case we performed three trajectories corresponding to three different values of q: 0.9, 0 and -1. In figure 4 we only display the results related to the case of $q = 0.9$ (figures $4a$, $4c$ and $4e$) and $q = -1$ (figures $4b$, $4d$ and $4f$). In particular, figures $4a$ and $4b$ display the observation functions with the nodes (red stars), figures $4c$ and $4d$ display the functions $\sigma(s_c)$ and figures $4e$ and $4f$ display the observation functions as observed (blue points), as estimated by our strategy alone (red points) and improved with the Levenberg Marquadt algorithm (black points) as explained in section 7. We remarked that the difference between the red and the black line is actually due to a poor estimation of the parameter k (obtained by using equation (36), i.e. by only using the two observations which are the closest to the mirror points). However, as explained in section 7 our strategy only needs to estimate the values of L and ξ_q for at least three trajectories and therefore the Levenberg Marquadt algorithm which only improves the estimation of k is actually unnecessary.

Figure 5 displays the same results shown in figure 4 but when the bearing sensor is very noisy ($\sigma_\beta = 5deg$). In this case the minimum of $\sigma(s_c)$ is significantly larger than 0 (figures $5c$ and $5d$).

By combining the estimated ξ_q and L for the three considered robot trajectories (i.e. with $q = 0.9,\ 0,\ -1$) we finally estimate the five parameters ϕ, ψ, η, δ and ξ. In table 3 we provide the values obtained for different errors on the bearing sensor (i.e. $\sigma_\beta = 1,\ 3,\ 5\ deg$). Even with a large error on the bearing sensor($\sigma_\beta = 5deg$) it is possible to achieve an excellent accuracy. In

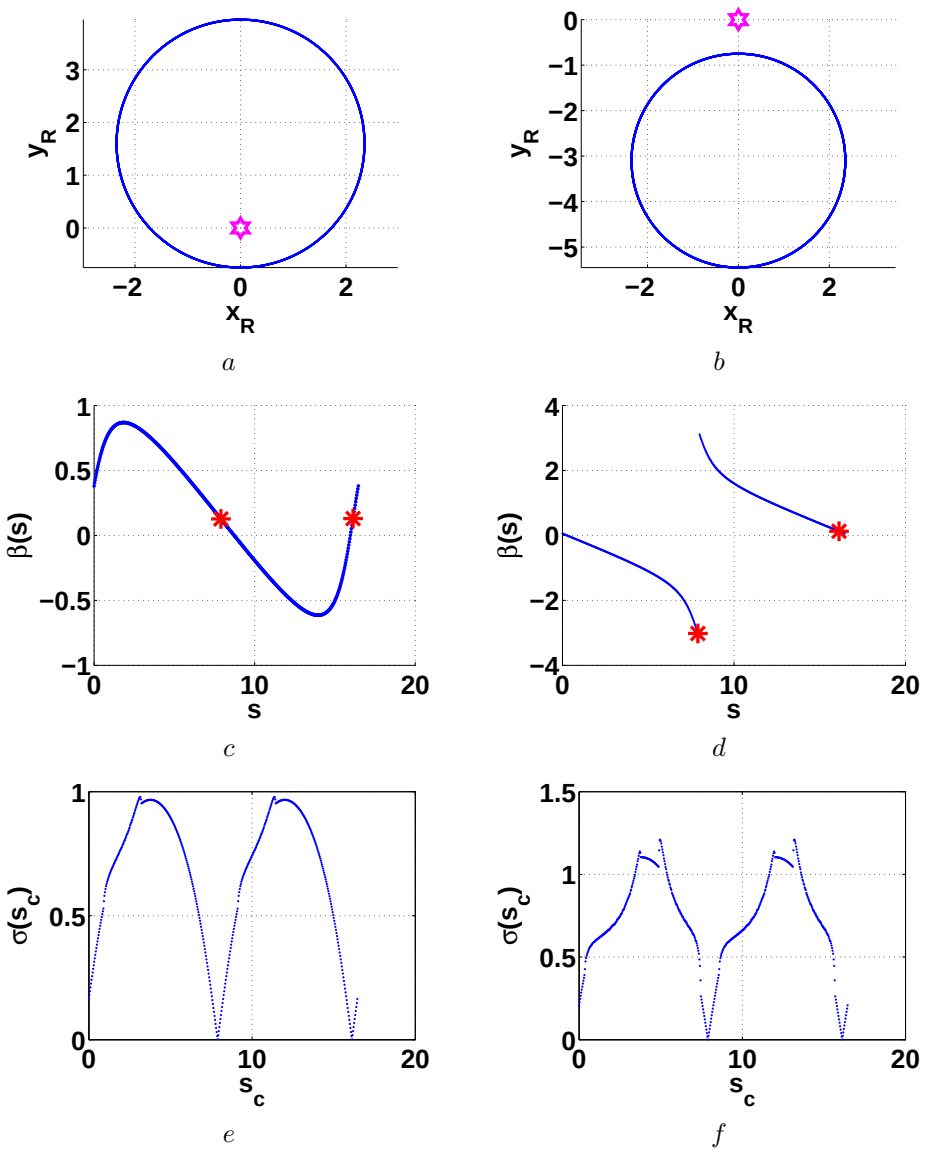

Figure 3: The phase of nodes detection in our strategy for the ideal case of perfect sensors and $q = 0.8$. a, c and e refer to the case when the feature is inside the accomplished trajectory while b, d and f when it is outside . a and b display the trajectories, c and d display the observation functions with the estimated nodes and e and f display the functions $\sigma(s_c)$.

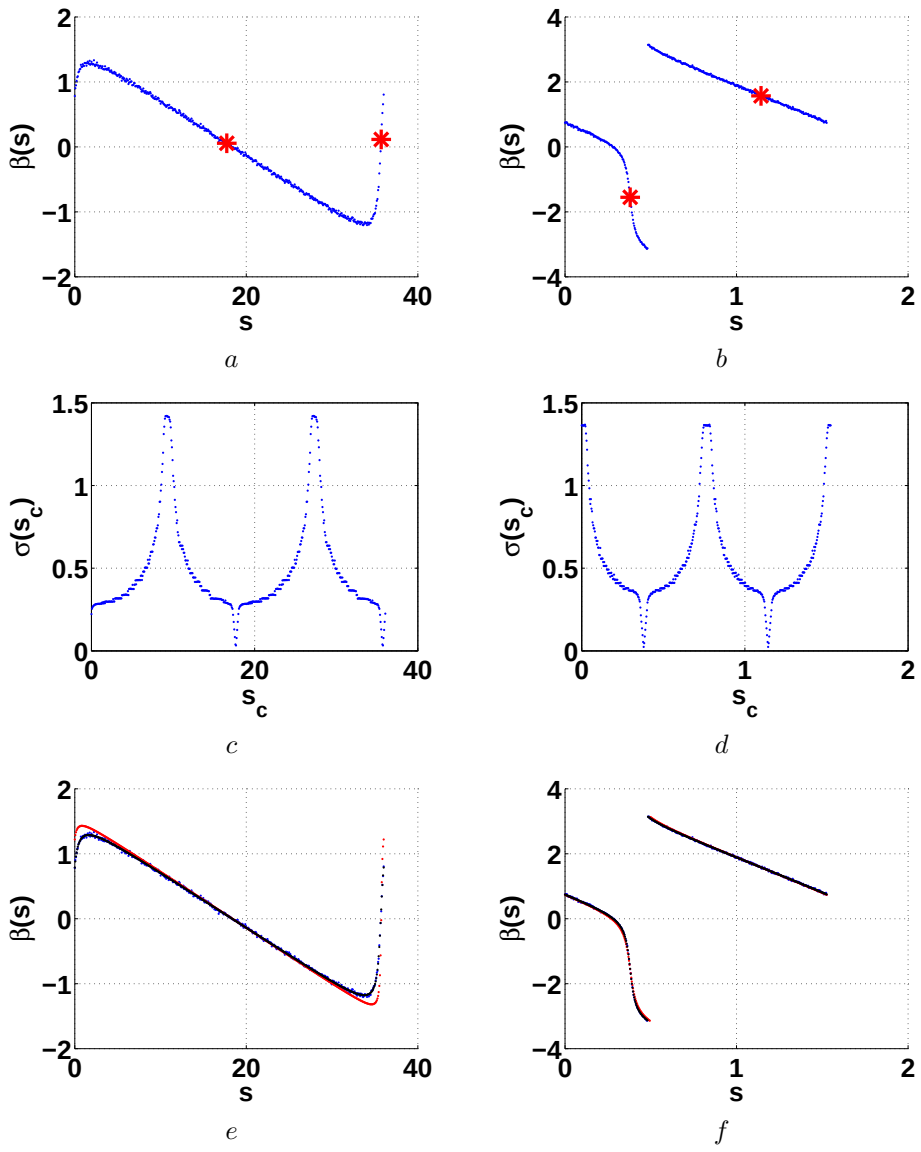

Figure 4: The estimation of the nodes and then the parameters ξ_q, L, c and k for $q = 0.9$ (a, c and e) and $q = -1$ (b, d and f). $\sigma_\beta = 1deg$ and $k = 0.001m^{\frac{1}{2}}$. a and b display the observation functions with the estimated nodes, c and d display the functions $\sigma(s_c)$ and e and f display the observation functions as observed (blue dots), as estimated by our strategy alone (red dots) and improved with the Levenberg Marquadt algorithm (black dots).

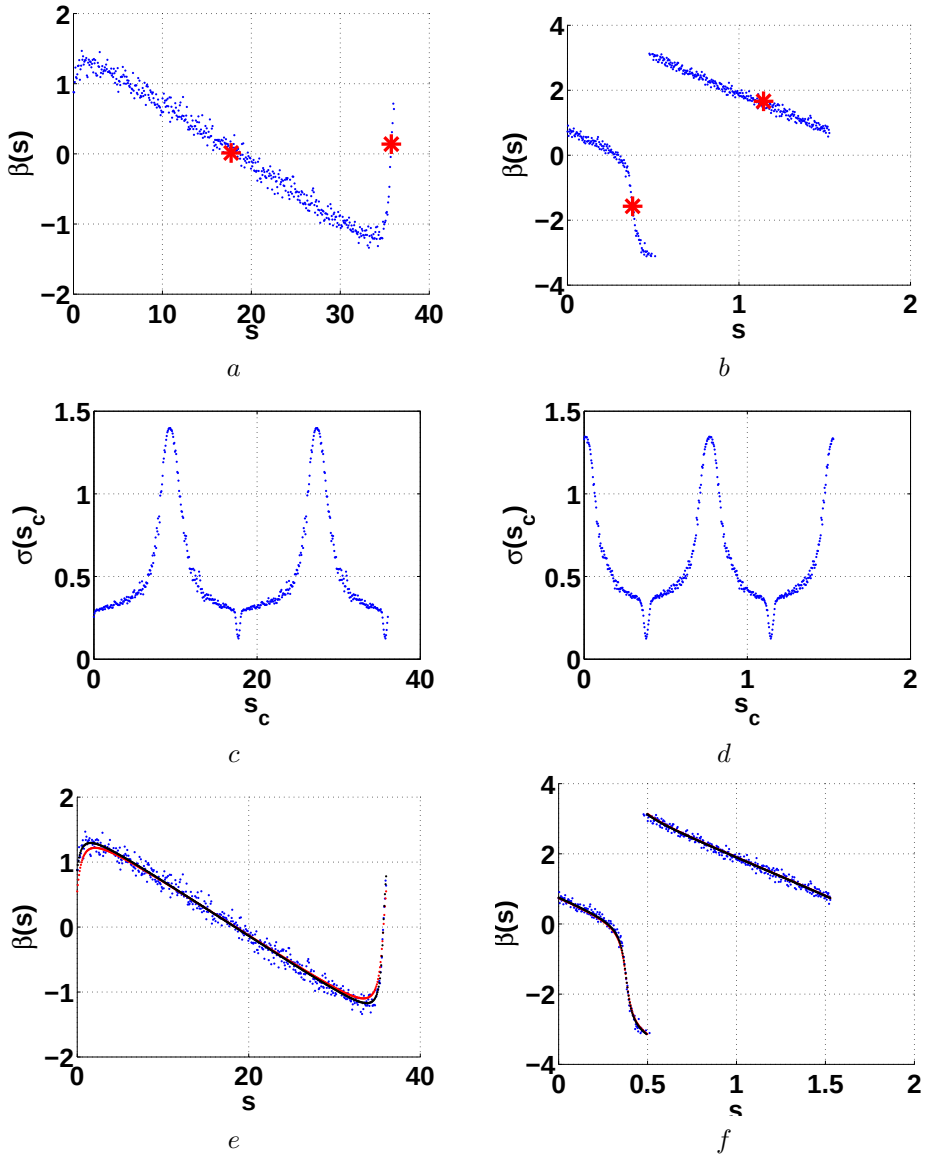

Figure 5: As in figure 4 but with a larger error on the bearing sensor ($\sigma_\beta = 5deg$).

σ_β	$\phi\ (deg)$	$\psi\ (deg)$	$\eta\ (m^{-1})$	δ	$\xi\ (m^{-1})$
True	0.00	90.0	1.6500	1.01616	2.0412
$1deg$	-0.08	90.05	1.6532	1.01610	2.0432
$3deg$	0.21	90.08	1.6454	1.01629	2.0389
$5deg$	0.13	89.83	1.6701	1.01607	2.0441

Table 3: The values of the calibration parameters adopted in our simulation. True values (first line) and estimated values for different σ_β.

σ_β	$\Delta\phi\ (deg)$	$\Delta\psi\ (deg)$	$\frac{\Delta\eta}{\eta}$	$\frac{\Delta\delta}{\delta}$	$\frac{\Delta\xi}{\xi}$
$1deg$	0.10	0.08	$3.2\ 10^{-3}$	$5.0\ 10^{-5}$	$4.5\ 10^{-4}$
$3deg$	0.19	0.13	$5.3\ 10^{-3}$	$1.2\ 10^{-4}$	$8.7\ 10^{-4}$
$5deg$	0.28	0.23	$8.5\ 10^{-3}$	$1.9\ 10^{-4}$	$1.3\ 10^{-3}$

Table 4: The errors on the estimated parameters averaged on 100 simulations for three different σ_β.

particular, the accuracy on the parameter δ is unbelievable (the relative error is smaller than 0.01% when $\sigma_\beta = 1deg$). We also remark that in our simulation the robot accomplishes the circular trajectory only once. It is possible to further improve the accuracy by moving the robot along more than one loop for every q and/or by considering more than three values of q. Table 3 refers to a single simulation. In order to have a more indicative result we performed 100 complete simulations obtaining 100 values for every estimated parameters. We compute the error on the estimated parameters for every simulation. In table 4 we report the mean value for these errors. It is possible to see that the relative error on the estimated parameters is particularly small (regarding δ is 0.005% when $\sigma_\beta = 1deg$)). We consider this an excellent result.

8.2 Real Experiments

To evaluate the performance of our strategy in a real case we used the mobile robot e-puck (see [9] for a detailed description of this robot and its sensors). In our experiments we only used the camera and the odometry sensors. Actually, our strategy has been developed to calibrate an omnidirectional bearing sensor. In contrast, the available camera, has a very limited overture ($\simeq 38deg$). In practice, it is in general not possible to observe a single feature during the entire circular trajectory accomplished by the robot. The only situation where this is possible occurs when the feature is inside the circular trajectory (as represented in figure 3a) and close to the center. Furthermore, the camera must look towards the center of the circumference. This is the case when the angle ϕ is close to $0deg$ and ψ is close to $90deg$). Since the available camera looks ahead, we fixed in front of the robot a small mirror (see figure 6). Obviously, in these conditions our strategy cannot estimate the extrinsic calibration parameters related to the real camera. However, it estimates the parameters related to the virtual camera, i.e. the one mirrored. We remark that the goal of this experiment is not to estimate the configuration of the true camera but to validate our strategy.

Therefore, we never mind whether the camera we are considering is the virtual camera.

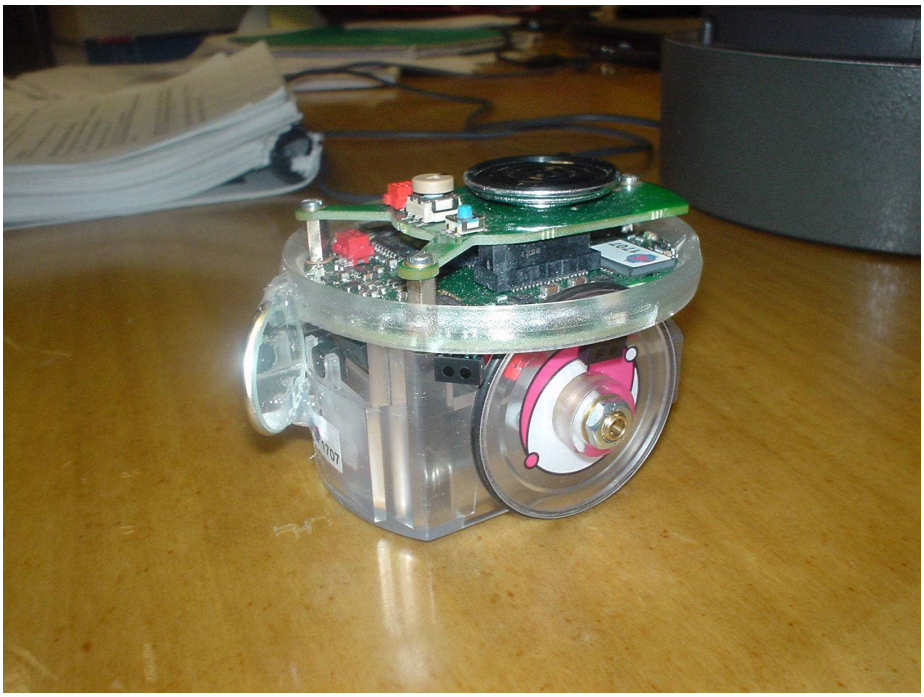

Figure 6: The robot e-puck with a small mirror in front of the camera.

An issue which arises when the feature is inside the trajectory is the possibility to have collisions with the feature. In order to avoid this, the circumference has to be large. In practice we could not consider trajectories with values of q smaller than 0.4.

The robot camera provides images with resolution 60×60. Figure 7a shows the robot e-puck together with the source of light we adopted as a point feature in our experiments. Figure 7b is an image of the feature taken by the e-puck camera during our experiments. The images were provided at a frequency in the range $[0.5, 8]Hz$.

We carried out two complete experiments. In the latter we increased the radius of the right wheel with a peace of tape. Each experiment consists of four independent trajectories with the following values of q: 0.9, 0.7, 0.6, 0.4. Regarding the estimation of the parameters ξ_q, L, c and k we show in figure 8 only the results related to the case $q = 0.6$ without tape. As for the simulations, we show the observation function with the estimated nodes (8a), the function $\sigma(s_c)$ (8b) and the observation functions as observed (blue points), as estimated by our strategy alone (red points) and improved with the Levenberg Marquadt algorithm (black points) (8c).

Table 5 reports the values of the parameters ξ_q, L, c and k obtained in our experiments for the different trajectories (i.e. the four considered values of q) with and without the tape on the right wheel. From these values we obtain the calibration parameters with and without tape reported in table 6. Regarding the

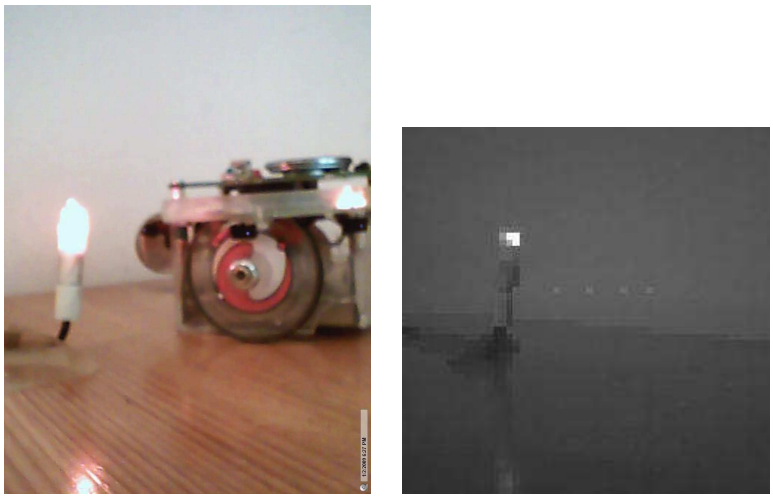

a *b*

Figure 7: The robot e-puck and the source of light used as the feature (a) and the feature observed by the robot camera (b).

	No	Tape		
q	ξ_q	L	c	k
0.9	1.9211	1.8469	−1.4644	1.9474
0.7	5.7110	1.6382	−1.2599	6.0827
0.6	7.5937	1.5291	−1.1587	8.0819
0.4	11.4347	1.3145	−.9850	11.6104
	With	Tape		
q	ξ_q	L	c	k
0.9	1.9666	1.8435	−1.4703	2.0027
0.7	5.7252	1.6355	−1.2845	6.1469
0.6	7.6559	1.5279	−1.1457	8.1331
0.4	11.4092	1.3103	−0.9737	11.5967

Table 5: The values of ξ_q, L, c and k obtained in our experiments for the considered trajectories.

Tape	ϕ (deg)	ψ (deg)	η (m^{-1})	δ	ξ (m^{-1})
No	−5.80	117.18	10.21	0.9987	18.99
Yes	−5.67	116.91	10.40	0.9959	18.97

Table 6: The calibration parameters with and without tape estimated in our experiments.

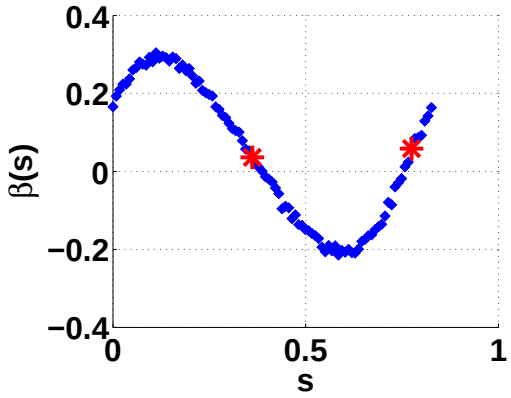

a

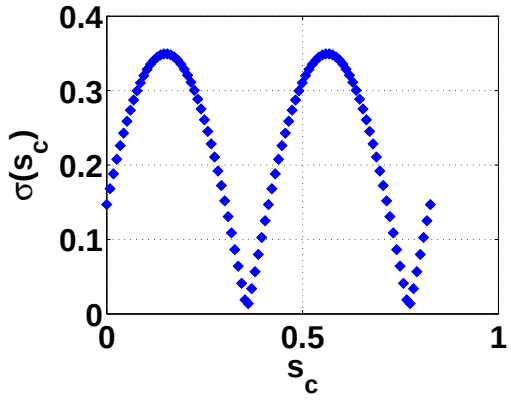

b

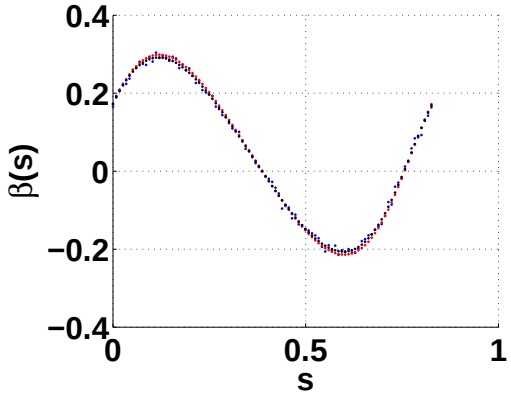

c

Figure 8: The estimation of the nodes and then the parameters ξ_q, L, c and k for $q = 0.6$ for the robot e-puck without tape. *a* displays the observation function with the estimated nodes, *b* displays the function $\sigma(s_c)$ and *c* displays the observation function as observed (blue points), as estimated by our strategy alone (red points) and improved with the Levenberg Marquadt algorithm (black points).

angles ϕ and ψ, we remark that the difference between the case with tape and without tape is smaller than $0.3deg$, which is roughly the mean errors obtained in our simulations (see the second and third column of table 4). This is consistent with the fact that the tape does not affect these angle parameters. On the other hand, we remark a significant difference for the parameters η and δ. Regarding η the difference is $\simeq 2\%$ which is larger than the mean error obtained in our simulations (see the fourth column of table 4). Regarding δ the difference is $\simeq 0.3\%$ which is larger than the mean error obtained in our simulations (see the fifth column of table 4). This is consistent with the increased radius of the right wheel due to the tape. The variation in the parameter ξ is very small and not in the expected direction. In particular, it is $\simeq 0.1\%$ which is roughly the mean error obtained in our simulations (see the last column of table 4). This parameter should be affected by the tape since it depends on δ_R. We believe that the tape also increased the effective distance between the wheels (i.e. the parameter δ_B) making $\xi = \frac{1}{B}\frac{\delta_R}{\delta_B}$ unaffected by the tape.

9 Conclusions

In this document we considered the problem of simultaneously calibrating an odometry system and the extrinsic parameters of a bearing sensor. The calibration only uses a single point feature.

Two new contributions were provided:

- A local decomposition of the considered system based on the theory of distributions developed in [12];
- A simple strategy to robustly, efficiently and accurately estimate the parameters describing both the extrinsic bearing sensor calibration and the odometry calibration.

The first contribution represents the first application of the distribution theory in the field of mobile robotics and the first non-trivial application of this theory to face a real estimation problem. In the specific case, it allowed us to detect for suitable trajectories the observable combinations of the original parameters describing our calibration problem.

By carrying out this decomposition for suitable circular trajectories, it was possible to analytically derive the expression of the bearing angle of the feature in the bearing sensor local frame vs the curve length of the robot trajectory as evaluated by the uncalibrated odometry. By analytically analyzing this expression it was possible to detect symmetry properties which play a very practical importance. Indeed, by only evaluating the axis of symmetry of this function and its period it is possible to immediately evaluate the observable combinations. Then, by performing at least three independent circular trajectories, it is possible to evaluate all the parameters describing our calibration problem.

The performance of the proposed strategy was carefully evaluated by carrying out both simulations and real experiments with the mobile robot e-puck. In both cases, we found excellent results in terms of precision, robustness and facility of implementation.

Future works will focus on the following topics:

- extend this strategy to the $3D$ case, i.e. remove the hypothesis of a perfect alignment of the vertical axis of the bearing sensor with the world frame vertical axis;
- extend this strategy in order to consider also range sensors and other kind of features.

References

[1] G. Antonelli and S. Chiaverini, Linear estimation of the physical odometric parameters for differential-drive mobile robots, Autonomous Robot, Vol 23, pages 59-68

[2] Bicchi A., Pratichizzo D., Marigo A. and Balestrino A., On the Observability of Mobile Vehicles Localization, IEEE Mediterranean Conference on Control and Systems, 1998

[3] Bonnifait P. and Garcia G., Design and Experimental Validation of an Odometric and Goniometric Localization System for Outdoor Robot Vehicles, IEEE Transaction On Robotics and Automation, Vol 14, No 4, August 1998

[4] Borenstein J., Feng L., "Measurement and correction of systematic odometry errors in mobile robots," *IEEE Transactions on Robotics and Automation*, vol. 12, pp. 869–880, 1996.

[5] X. Brun and F. Goulette, Modeling and calibration of coupled fisheye CCD camera and laser range scanner for outdoor environment reconstruction, in Proceedings of the International Conference on 3D Digital Imaging and Modeling, Montreal, QC, Canada, Aug. 2123, 2007, pp. 320327.

[6] Caltabiano D., Muscato G. and Russo F., "Localization and Self Calibration of a Robot for Volcano Exploration" *International Conference on Robotics and Automation*, pp. 586–591, New Orleans, USA, 2004.

[7] Chong K.S., Kleeman L., "Accurate Odometry and Error Modelling for a Mobile Robot," *International Conference on Robotics and Automation*, vol. 4, pp. 2783–2788, 1997.

[8] Doh, N. L., Choset, H. and Chung, W. K., Relative localization using path odometry information, Autonomous Robots, Vol 21, pages 143-154

[9] http://www.e-puck.org/

[10] E.M. Foxlin, Generalized Architecture for Simultaneous Localization, Auto-Calibration, and Map building, International Conference on Intelligent Robots and Syrtems, EPFL, Switzerland, October 2002.

[11] Hermann R. and Krener A.J., 1977, Nonlinear Controllability and Observability, IEEE Transaction On Automatic Control, AC-22(5): 728-740

[12] Isidori A., Nonlinear Control Systems, 3rd ed., Springer Verlag, 1995.

[13] Larsen, T.D., Hansen K.L., Andersen N.A. and Ole Ravn, Design of Kalman filters for mobile robots; evaluation of the kinematic and odometric approach, Proceedings of the 1999 IEEE International conference on Control Applications, volume: 2 , 22-27 Aug. 1999, Pages:102l-1026.

[14] Martinelli A, "The odometry error of a mobile robot with a synchronous drive system", *IEEE Trans. on Robotics and Automation* Vol 18, NO. 3 June 2002, pp 399–405

[15] A. Martinelli, N. Tomatis and R. Siegwart, Simultaneous Localization and Odometry Self Calibration for Mobile Robots, Autonomous Robot, Vol 22 Issue 1, January 2007, pages 75-85

[16] A. Martinelli, D. Scaramuzza and R. Siegwart, Automatic Self-Calibration of a Vision System during Robot Motion, International Conference on Robotics and Automation, Orlando, Florida, April 2006.

[17] A. Martinelli and R. Siegwart, Observability Properties and Optimal Trajectories for On-line Odometry Self-Calibration. In Proceedings of IEEE International Conference on Decision and Control, San Diego, California, December 2006.

[18] A. Martinelli, Local Decomposition and Observability Properties for Automatic Calibration in Mobile Robotics, to be presented at the International Conference on Robotics and Automation, Kobe, Japan, May 2009.

[19] F. M. Mirzaei and S. I. Roumeliotis, A Kalman filter-based algorithm for IMU-camera calibration: Observability analysis and performance evaluation, IEEE Transactions on Robotics, 2008, Vol. 24, No. 5, October 2008, pages 1143-1156

[20] Roy N., and Thrun S., Online Self-calibration for Mobile Robots, proceedings of the 1999 IEEE International Conference on Robotics and Automation, 19 May 1999 Detroit, Michigan, pp. 2292-2297.

[21] H.J. von der Hardt, R. Husson, D. Wolf, An Automatic Calibration Method for a Multisensor System: Application to a Mobile Robot Localization System, Interbational Conference on Robotics and Automation, Leuven, Belgium, May 1998.

[22] S. Wasielewski and O. Strauss, Calibration of a multi-sensor system laser rangefinder/camera, in Proceedings of the Intelligent Vehicles Symposium, Detroit, MI, Sept. 2526, 1995, pp. 472477.

[23] Q. Zhang and R. Pless, Extrinsic calibration of a camera and laser range finder (improves camera calibration), in Proceedings of the IEEE/RSJ International Conference on Intelligent Robots and Systems, Sendai, Japan, Sept. 28Oct. 2, 2004, pp. 23012306.

10 Appendix

A: Observability for the system defined by equation (6)

Let us refer to the system whose dynamics and observation are defined in (6). Accordingly with the rank criterion, we have to provide five Lie derivatives whose gradients span the entire configuration space. Let us consider the matrix whose lines are the gradients of the Lie derivatives $L^0\beta$, $L^1_{f_1}\beta$, $L^1_{f_2}\beta$, $L^2_{f_1f_1}\beta$, $L^2_{f_1f_2}\beta$, $L^2_{f_2f_1}\beta$ and $L^2_{f_2f_2}\beta$, where f_1 and f_2 are defined in (8). The determinant of this matrix is: $-16\delta^4\mu^5\eta^3\xi^5\cos(\gamma-\phi)(\mu\cos\phi-\cos(\gamma-\phi))/(\mu^2+2\mu\cos\gamma+1)^5$ which is in general different from 0.

B: Local Decomposition for the system defined by equation (12)

By applying the distribution theory as developed in [12], we have to solve a system of partial differential equations (see the first chapter in [12]). However, the partial differential equations associated to the system defined in (12) are too complicated and analytically deriving their solutions is too hard. For this reason, we proceed in two separate steps. We first consider the following simpler system:

$$\begin{cases} \dot{\mu} &= -\mu^2\eta_q\nu\cos(\gamma-\phi) \\ \dot{\gamma} &= \xi_q\nu - \mu\eta_q\nu\sin(\gamma-\phi) \\ \dot{\eta}_q &= \dot{\xi}_q = \dot{\phi} = 0 \\ y &= \dfrac{\sin\gamma}{\mu+\cos\gamma} \end{cases} \tag{A.1}$$

where we removed the variable ψ. We apply the method developed in [12] in order to find the local decomposition for this simplified system.

The associated partial differential equation is in this case:

$$(\mu\cos\gamma+1)\frac{\partial\Psi}{\partial\mu} + \sin\gamma\frac{\partial\Psi}{\partial\gamma} + \frac{\xi_q\cos\phi}{\eta_q\mu}\frac{\partial\Psi}{\partial\phi} + \frac{\xi_q\sin\phi-\eta_q}{\mu}\frac{\partial\Psi}{\partial\eta_q} = 0$$

namely, every solution $\Psi(\mu,\gamma,\phi,\eta_q,\xi_q)$ of the previous partial differential equation is an observable quantity for the system in (A.1). We found the follow-

ing four independent solutions: $\Psi_1^q = \frac{\xi_q - \eta_q \sin\phi}{\eta_q \cos\phi}$, $\Psi_2^q = \frac{\mu\eta_q \cos\phi}{\sin\gamma}$, $\Psi_3 = \frac{\mu + \cos\gamma}{\sin\gamma}$, $\Psi_4^q = \xi_q$. The local decomposition of (A.1) is:

$$\begin{cases} \dot{\Psi}_1^q = 0 \\ \dot{\Psi}_2^q = \nu\Psi_2^q(\Psi_1^q\Psi_2^q - \Psi_4^q\Psi_3) \\ \dot{\Psi}_3 = \nu(\Psi_2^q + \Psi_1^q\Psi_2^q\Psi_3 - \Psi_4^q - \Psi_4^q\Psi_3^2) \\ \dot{\Psi}_4^q = 0 \\ y = \dfrac{1}{\Psi_3} \end{cases} \tag{A.2}$$

Let us proceed with the second step. We add to the system in (A.2) the parameter ψ (with $\dot{\psi} = 0$) and we consider the output $y = -atan\left(\frac{1}{\Psi_3}\right) - \psi$ instead of $y = \frac{1}{\Psi_3}$. We apply again the method in [12] on the resulting system. The associated partial differential equation is in this case:

$$(\Psi_1^{q^2} + 1)\frac{\partial G}{\partial \Psi_1^q} + (\Psi_2^q(\Psi_3 - \Psi_1^q))\frac{\partial G}{\partial \Psi_2^q} + (\Psi_3^2 + 1)\frac{\partial G}{\partial \Psi_3} + \frac{\partial G}{\partial \psi} = 0$$

namely, every solution $G(\Psi_1^q, \Psi_2^q, \Psi_3, \Psi_4^q, \psi)$ of the previous partial differential equation is an observable quantity for this resulting system. We found the following four independent solutions: $A^q = \frac{\Psi_1^q - \Psi_3}{1 + \Psi_1^q\Psi_3}$, $V^q = \Psi_2^q \frac{1 + \Psi_1^q\Psi_3}{1 + \Psi_3^2}$, $L^q = \psi - atan\Psi_1^q$ and Ψ_4^q. The local decomposition is given in (14).

Contents

Centre de recherche INRIA Grenoble – Rhône-Alpes
655, avenue de l'Europe - 38334 Montbonnot Saint-Ismier (France)

Centre de recherche INRIA Bordeaux – Sud Ouest : Domaine Universitaire - 351, cours de la Libération - 33405 Talence Cedex
Centre de recherche INRIA Lille – Nord Europe : Parc Scientifique de la Haute Borne - 40, avenue Halley - 59650 Villeneuve d'Ascq
Centre de recherche INRIA Nancy – Grand Est : LORIA, Technopôle de Nancy-Brabois - Campus scientifique
615, rue du Jardin Botanique - BP 101 - 54602 Villers-lès-Nancy Cedex
Centre de recherche INRIA Paris – Rocquencourt : Domaine de Voluceau - Rocquencourt - BP 105 - 78153 Le Chesnay Cedex
Centre de recherche INRIA Rennes – Bretagne Atlantique : IRISA, Campus universitaire de Beaulieu - 35042 Rennes Cedex
Centre de recherche INRIA Saclay – Île-de-France : Parc Orsay Université - ZAC des Vignes : 4, rue Jacques Monod - 91893 Orsay Cedex
Centre de recherche INRIA Sophia Antipolis – Méditerranée : 2004, route des Lucioles - BP 93 - 06902 Sophia Antipolis Cedex

Éditeur
INRIA - Domaine de Voluceau - Rocquencourt, BP 105 - 78153 Le Chesnay Cedex (France)
http://www.inria.fr
ISSN 0249-6399